

Perturbative Frequency Expansion for Nearly Monochromatic Binary Black Holes Detectable with LISA

Naoki Seto

Department of Physics, Kyoto University, Kyoto 606-8502, Japan

(Dated: June 21, 2024)

The proposed space gravitational wave (GW) detector LISA has potential to detect stellar-mass black hole binaries (BBHs). The majority of the detected BBHs are expected to emit nearly monochromatic GWs, whose frequency evolution will be efficiently described by Taylor expansions. We study the measurability of the associated time derivative coefficients of the frequencies, by extending a recent work based on a simplified Fisher matrix analysis. Additionally, we provide qualitative discussions on how to extract astrophysical information, such as orbital eccentricity and tertiary perturbation, from the observed derivative coefficients.

I. INTRODUCTION

The LIGO-Virgo-Kagra network had detected $O(100)$ binary black holes (BBHs) by the end of its O3 run [1]. The proposed space GW detectors such as LISA [2], Taiji [3] and TianQin [4] can observe similar BBHs in the lower frequency regime [5, 6].

According to a recent statistical analysis employing the LVK GWTC-3 catalog, LISA is expected to detect $N_{\text{tot}} \sim 2.3(T/4\text{yr})^{3/2}(\rho_{\text{thr}}/10)^{-3}$ BBHs similar to those cataloged [7] (see also [8, 9] for multiband observations). Here ρ_{thr} is the detection threshold for the signal-to-noise ratio, and T is the observational period. The estimated number N_{tot} contains an uncertainty of a factor of two, partly due to the unclear redshift dependence of the merger rate. In the statistical analysis, the BBHs are simply assumed to be nearly circular still in the LISA band.

In the total number N_{tot} , the fraction of BBHs that will merge in the observational period $T = 4\text{yr}$ was estimated to be $\sim 5\%$ ($\sim 10\%$ for $T = 10\text{yr}$) [7]. In fact, the majority of the detected BBHs will be nearly monochromatic GW sources, with the peak number density (per logarithmic frequency interval) around $f \sim 5\text{mHz}$. Here the characteristic frequency $\sim 5\text{mHz}$ is given as the tangential point of the noise spectrum $S_n(f)$ with the slope $f^{-2/9}$ which is derived from the radiation reaction. In [7], the median chirp mass of the detected BBHs was also estimated to be $\mathcal{M} \sim 30M_\odot$ with a relatively large uncertainty for the distribution function at $\mathcal{M} \gtrsim 50M_\odot$.

For the nearly monochromatic GWs from these BBHs, we will be able to efficiently describe the frequency evolution, using the time derivative coefficients \dot{f}, \ddot{f}, \dots (also denoting $f^{(n)} = \partial_t^n f$), as conventionally applied in similar occasions (e.g. spin-down of a pulsar). This approach condenses the evolutionary information to a finite number of parameters and will be mathematically more tractable, rather than directly dealing with the functional degrees of freedom. Meanwhile, stimulated by the recent reports on the long-term orbital evolution of HM Cancri (an interacting double white dwarf binary at $f = 6.2\text{mHz}$) [10, 11], the author developed a simplified Fisher matrix analysis on the estimation errors of the fre-

quency derivatives up to the second order \ddot{f} [12] (see also [13]). In this paper, extending the analytical approach to include higher derivatives such as \dot{f} and beyond, we apply it to the nearly monochromatic BBHs in the LISA band.

Importantly, compared with the BBHs in the LVK band, those in the LISA band could have much larger eccentricities [14–16]. Likewise, in the LISA band, the environmental effects (e.g. tertiary perturbation) could be more strongly imprinted in the emitted GWs, because of the longer gravitational radiation timescale [17–26]. In this paper, we also discuss the possibilities of examining the orbital eccentricities and the potential tertiary perturbations from the observables $f, \dot{f}, \ddot{f}, \dots$ (see also [27]). To this end, we introduce the non-dimensional parameters $C_n \propto f^{(n)} f^{n-1} / (\dot{f})^n$ ($n = 2, 3, \dots$) which are adjusted to be $C_n = 1$ for an isolated circular BBH. We apply Fisher matrix results to evaluate the measurement errors for the parameters C_n .

To provide a concrete picture for our study, we consider an equal mass BBH with the characteristic values mentioned earlier: a chirp mass $\mathcal{M} = 30M_\odot$, a GW frequency $f = 5\text{mHz}$ and a signal strength $\rho = 10$ (for $T = 4\text{yr}$ with LISA). We set this BBH as our fiducial observational target.

This paper is organized as follows. In section II, we evaluate the frequency derivatives $f^{(n)}$ for circular and eccentric BBHs. We introduce the non-dimensional measures C_n and qualitatively argue the corrections due to tertiary perturbations. In section III, based on the Fisher matrix analysis, we present analytical expressions for the estimation errors of the time derivatives $f^{(n)}$. In section IV, we discuss the measurability of these derivative coefficients. We relatedly discuss the prospects for studying orbital eccentricity and tertiary effects by using the quantities C_n . In section V, we mention potential extensions of this study. Section VI is a brief summary of this paper.

TABLE I: Fiducial binary parameters and the associated frequency derivatives due to the radiation reaction for a circular orbit.

frequency f	5 mHz
chirp mass \mathcal{M}	$30 M_\odot$
SNR ρ (4yr)	10
\dot{f}	$6.2 \times 10^{-13} \text{Hz s}^{-1}$
\ddot{f}	$2.8 \times 10^{-22} \text{Hz s}^{-2}$
\dddot{f}	$2.2 \times 10^{-31} \text{Hz s}^{-3}$
$\overset{\cdot\cdot\cdot}{f}$	$2.4 \times 10^{-40} \text{Hz s}^{-4}$

II. EVOLUTION OF BINARY BLACK HOLES

A. Circular Systems

Let us first discuss the orbital evolution of a circular BBH. In the quadrupole approximation, the chirp rate of the GW frequency f (twice the orbital frequency) is given by

$$\frac{df}{dt} = \frac{96\pi^{8/3} G^{5/3} \mathcal{M}^{5/3} f^{11/3}}{5c^5} \quad (1)$$

with the chirp mass \mathcal{M} , the gravitational constant G and the speed of light c [14]. For our fiducial model parameters (summarized in Table 1) we have

$$\dot{f} = 6.2 \times 10^{-13} \left(\frac{\mathcal{M}}{30M_\odot} \right)^{5/3} \left(\frac{f}{5\text{mHz}} \right)^{11/3} \text{Hz s}^{-1}. \quad (2)$$

Correspondingly, in the observational period T , the GW frequency f increases only by $1.5(T/4\text{yr})$ percent.

Recursively taking the time derivatives of Eq. (1), we can readily obtain the higher time derivatives such as

$$\ddot{f} = 2.8 \times 10^{-22} \left(\frac{\mathcal{M}}{30M_\odot} \right)^{10/3} \left(\frac{f}{5\text{mHz}} \right)^{19/3} \text{Hz s}^{-2}, \quad (3)$$

$$\dddot{f} = 2.2 \times 10^{-31} \left(\frac{\mathcal{M}}{30M_\odot} \right)^5 \left(\frac{f}{5\text{mHz}} \right)^9 \text{Hz s}^{-3}, \quad (4)$$

$$\overset{\cdot\cdot\cdot}{f} = 2.4 \times 10^{-40} \left(\frac{\mathcal{M}}{30M_\odot} \right)^{20/3} \left(\frac{f}{5\text{mHz}} \right)^{35/3} \text{Hz s}^{-4}. \quad (5)$$

By integrating Eq. (1), we can also estimate the time before the merger as

$$t_c = 97 \left(\frac{\mathcal{M}}{30M_\odot} \right)^{-5/3} \left(\frac{f}{5\text{mHz}} \right)^{-8/3} \text{yr}. \quad (6)$$

In terms of t_c , the time derivatives are roughly given by

$$\partial_t^n f = f^{(n)} \sim \frac{f}{t_c^n}. \quad (7)$$

More precisely, from Eq. (1), we can show

$$C_2 \equiv \frac{3\ddot{f}f}{11\dot{f}^2} = 1, \quad (8)$$

$$C_3 \equiv \frac{9\ddot{f}f^2}{209\dot{f}^3} = 1, \quad (9)$$

$$C_4 \equiv \frac{\overset{\cdot\cdot\cdot}{f}f^3}{209\dot{f}^4} = 1. \quad (10)$$

Up to now, we ignored the post-Newtonian effects. The leading order (1PN) correction to the product C_2 takes a negative value [28, 29]

$$-\frac{2}{11} \left(\frac{743}{336} + \frac{11\eta}{4} \right) \left(\frac{GM_t \pi f}{c^3} \right)^{2/3} \quad (11)$$

with the symmetric mass ratio η and the total mass $M_t = \eta^{-3/5} \mathcal{M}$. In the LISA era, from the preceding ground based detectors including the Einstein Telescope [30], we will be able to use the detailed prior information on the ratio η for stellar mass BBHs and better model the PN corrections. For an equal mass binary (with $\eta = 1/4$), Eq. (11) is expressed as

$$-1.6 \times 10^{-4} \left(\frac{\mathcal{M}}{30M_\odot} \right)^{2/3} \left(\frac{f}{5\text{mHz}} \right)^{2/3}. \quad (12)$$

B. Eccentric Systems

Next we discuss the time evolution of an eccentric BBH (see also [31]). We continue to use f as twice the orbital frequency. At the quadrupole order, using the orbital eccentricity e , we can write down the evolution equations [14]

$$\begin{aligned} \frac{df}{dt} &= \frac{96\pi^{8/3} G^{5/3} \mathcal{M}^{5/3} f^{11/3}}{5c^5 (1-e^2)^{7/2}} \left(1 + \frac{73e^2}{24} + \frac{37e^4}{96} \right) \\ &\equiv F_1(f, e), \end{aligned} \quad (13)$$

$$\begin{aligned} \frac{de}{dt} &= -\frac{304\pi^{8/3} G^{5/3} f^{8/3} \mathcal{M}^{5/3} e}{15c^5 (1-e^2)^{5/2}} \left(1 + \frac{121e^2}{304} \right) \\ &\equiv E_1(f, e). \end{aligned} \quad (15)$$

Applying the chain rule for derivatives, we can evaluate the second derivative \ddot{f} as follows

$$\ddot{f} = \frac{\partial F_1}{\partial f} F_1 + \frac{\partial F_1}{\partial e} E_1 \equiv F_2(f, e). \quad (17)$$

The product C_2 in Eq. (8) is now given as

$$\begin{aligned} C_2 &= \frac{3\ddot{f}f}{11\dot{f}^2} \\ &= \frac{4(407e^8 + 2344e^6 + 93810e^4 + 58720e^2 + 25344)}{11(37e^4 + 292e^2 + 96)^2} \\ &\equiv K_2(e) \end{aligned} \quad (18)$$

$$(19)$$

with a perturbative expression

$$K_2(e) = 1 - \frac{2983e^2}{792} + O(e^4). \quad (20)$$

In contrast to Eqs. (13) and (15), the function $K_2(e)$ is regular at $e = 1$ with $K_2(1) = 4/11$.

In the same manner as Eq. (17), we can evaluate the third derivative \ddot{f} for an eccentric orbit as

$$\ddot{f} = \frac{\partial F_2}{\partial f} F_1 + \frac{\partial F_2}{\partial e} E_1 \equiv F_3(f, e). \quad (21)$$

We then evaluate the product C_3 and define the function $K_3(e)$

$$\begin{aligned} C_3 &= \frac{9 \ddot{f} f^2}{209 \dot{f}^3} \quad (22) \\ &= \frac{4}{209 (37e^4 + 292e^2 + 96)^3} (-9361e^{12} + 500532e^{10} \\ &\quad - 42206966e^8 + 145890160e^6 + 129278336e^4 \\ &\quad + 104147968e^2 + 46227456) \\ &\equiv K_3(e) \quad (23) \end{aligned}$$

with $K_3(0) = 1$, $K_3(1) = 20/209$ and

$$K_3(e) = 1 - \frac{2041e^2}{297} + O(e^4). \quad (24)$$

Likewise, we can evaluate the fourth derivative $\ddot{\ddot{f}}$ ($\equiv f^{(4)}$) and the product

$$C_4 = \frac{\ddot{\ddot{f}} f^3}{209 \dot{f}^4}. \quad (25)$$

The analytic expression for the corresponding function $K_4(e)$ is given as

$$\begin{aligned} K_4(e) &= \frac{8}{5643(37e^4 + 292e^2 + 96)^4} (421245e^{16} \\ &\quad - 100387440e^{14} + 12951727630e^{12} \\ &\quad - 122186028060e^{10} + 117746520816e^8 \\ &\quad + 132600265216e^6 + 150472180736e^4 \\ &\quad + 137985376256e^2 + 59910782976) \quad (26) \end{aligned}$$

with $K_4(0) = 1$, $K_4(1) = 40/1881$ and

$$K_4(e) = 1 - \frac{1898287e^2}{192456} + O(e^4). \quad (27)$$

In Fig. 1, we present the functions $K_2(e)$, $K_3(e)$ and $K_4(e)$. All of them decrease monotonically with e . By evaluating the products C_n from the observed frequency derivatives, we might inversely estimate the orbital eccentricity e .

The PN corrections to the products C_n depend on the eccentricity e . In this paper, we approximately use the results (12) also for mildly eccentric BBHs.

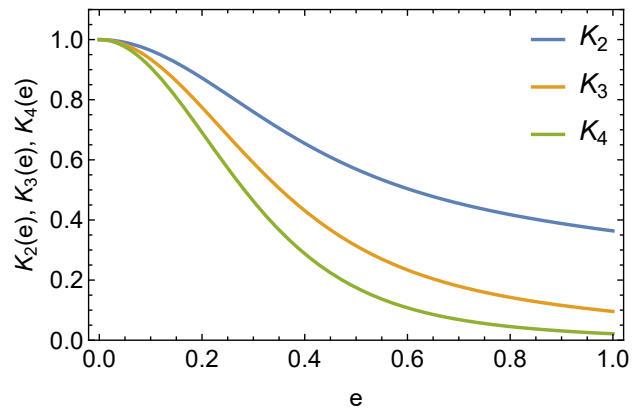


FIG. 1: The three functions $K_2(e)$, $K_3(e)$ and $K_4(e)$ defined in Eqs. (19) (23) and (26). For a circular binary ($e = 0$), we have $K_2 = K_3 = K_4 = 1$. At $e = 0.1$, we have $K_2 = 0.96$, $K_3 = 0.93$ and $K_4 = 0.91$.

C. Tertiary Effects

Here, we briefly discuss the GW phase modulation induced by a tertiary (of mass m_s) around a BBH (see, e.g. [32–34] for the effects on the derivative coefficients $f^{(n)}$), as a representative environmental perturbation. In this subsection, we temporarily attach the subscript s to the tertiary related quantities and r to the radiational effects (under the approximation ignoring the cross terms [32]). For simplicity, we assume that the outer orbits is hierarchical and circular with the period P_s and the semimajor axis R_s . We have

$$R_s = \left[\frac{G(M_t + m_s)P_s^2}{4\pi^2} \right]^{1/3}. \quad (28)$$

from the third Kepler law. In this simplified case, the BBH moves approximately on a circular orbit around the barycenter of the triple system.

Following [32], we briefly discuss the tertiary corrections (equivalent to the Rømer effects) to the apparent GW frequency and its derivative coefficients. The positional variation induces the phase shift as

$$\Phi_s(t) = -2\pi f_r D(t)/c \quad (29)$$

where $D(t)$ is the line-of-sight distance variation and expressed as (ϕ_s : the initial outer orbital phase)

$$D(t) = D_s \cos[2\pi t/P_s + \phi_s] \quad (30)$$

with the projected distance

$$D_s = \frac{m_s}{M_t + m_s} R_s \sin I_s \quad (31)$$

(I_s : the outer inclination angle). The tertiary corrections to the apparent GW frequency and its time derivatives are given as

$$f_s = \frac{1}{2\pi} \frac{d\Phi_s}{dt}, \quad \dot{f}_s = \frac{1}{2\pi} \frac{d^2\Phi_s}{dt^2}, \quad \ddot{f}_s = \frac{1}{2\pi} \frac{d^3\Phi_s}{dt^3} \quad (32)$$

and so on.

We put $v_s \sim 2\pi D_s/P_s$ as the line-of-sight component of the outer circular velocity of the binary. Then, for an observational time $T(\ll P_s)$, the tertiary effects $f_s^{(n)}$ have the characteristic magnitudes

$$|f_s^{(n)}| \sim f \left(\frac{v_s}{c}\right) \left(\frac{2\pi}{P_s}\right)^n. \quad (33)$$

A typical field system will have $v_s/c \ll 1$. Depending on the outer orbital phase, the tertiary corrections $f_s^{(n)}$ can take both signs.

Now we compare the tertiary and radiational effects, using Eqs. (7) and (33). We can roughly evaluate the ratios

$$\frac{|f_s^{(n)}|}{f_r^{(n)}} \sim \left(\frac{v_s}{c}\right) \left(\frac{2\pi t_c}{P_s}\right)^n \quad (34)$$

with the time t_c before the merger. For $2\pi t_c/P_s \gg 1$, the tertiary effects could be relatively more important at larger n . However, in contrast to Galactic white dwarf binaries ($t_c \gtrsim 10^5$ yr in the LISA band), our BBHs have much shorter merger time $t_c \sim 100$ yr, and the amplification factor $(2\pi t_c/P_s)$ will work less efficiently in Eq. (34).

As a concrete reference model, we set the tertiary mass $M_s \sim 25M_\odot$ and an edge-on outer orbit ($I_s = \pi/2$) of $P_s = 60$ yr ($\ll 2\pi t_c$). Then, using Eqs. (29)-(32), we obtain

$$\frac{f_s}{f_r} = 1.1 \times 10^{-4} \sin \psi_s, \quad (35)$$

$$\frac{\dot{f}_s}{\dot{f}_r} = 8.2 \times 10^{-4} \cos \psi_s, \quad (36)$$

$$\frac{\ddot{f}_s}{\ddot{f}_r} = -6.0 \times 10^{-3} \sin \psi_s, \quad (37)$$

$$\frac{\overset{\cdot\cdot\cdot}{f}_s}{\overset{\cdot\cdot\cdot}{f}_r} = -2.6 \times 10^{-2} \cos \psi_s \quad (38)$$

with the outer orbital phase parameter $\psi_s = 2\pi t/P_s + \phi_s$.

In this paper, we ignore the dynamical interaction between the inner and outer orbits (see, e.g. [35]). This would be a reasonable approximation for our reference tertiary system, at least for the Kozai-Lidov mechanism.

If the tertiary effects are much smaller than the radiational effects (as for the reference model above), we can perturbatively deal with the former. For $n = 2$, we have

$$C_2 = \frac{3(\ddot{f}_r + \ddot{f}_s)(f_r + f_s)}{11(\dot{f}_r + \dot{f}_s)^2} \simeq K_2(e) \left(1 + \frac{f_s}{f_r} - 2\frac{\dot{f}_s}{\dot{f}_r} + \frac{\ddot{f}_s}{\ddot{f}_r}\right) \quad (39)$$

and similarly

$$C_n \simeq K_n(e) \left(1 + (n-1)\frac{f_s}{f_r} - n\frac{\dot{f}_s}{\dot{f}_r} + \frac{f_s^{(n)}}{f_r^{(n)}}\right) \quad (40)$$

with the inequalities $K_n(e) \leq K_n(0) = 1$ from the definitions of $K_n(e)$. As shown in Eq. (40) The eccentricity and tertiary effects degenerate in the product C_n .

For a nearly circular binary $e \sim 0$, we could have a chance to observe the excess $C_n - 1 > 0$ due to the second factor in Eq. (40), depending on the outer orbital phase ψ_s . This inequality cannot be realized for an isolated eccentric BBH and suggests the existence of a third body, as one of its causes.

The situation will be more complicated for an eccentric binary, for which the tertiary effect might be actually more interesting in view of dynamical processes. In some cases, we will be able to measure the higher order product C_3 in addition to the lowest one C_2 . Then the orbital eccentricity e can be estimated independently for $n = 2$ and 3 by $e = K_n^{-1}(C_n)$. The tertiary effects could induce a mismatch between the inverted values. Note that we have $K'_n(0) = 0$, and the inversions work less efficiently for nearly circular binary $e \simeq 0$.

Below, in particular for the expected values for the frequency derivatives $f^{(n)}$, we mainly deal with the radiational effects, dropping the subscripts r and s (if unnecessarily). We will return to the tertiary effect later in Sec. IV D.

III. FISHER MATRIX ANALYSIS

In this section, we apply the Fisher matrix analysis to analytically evaluate how well we can measure the frequency derivatives in a matched filtering analysis for a nearly monochromatic BBH.

A. Simplified Waveform Model

We basically extend the earlier work by the author [12] (see also [22, 36]) and apply the simplified waveform model

$$h(t) = A \cos[\Phi_n(t)] \quad (41)$$

with the constant amplitude A and the phase function

$$\Phi_n(t) = 2\pi \left(ft + \frac{\dot{f}t^2}{2!} + \frac{\ddot{f}t^3}{3!} + \dots + \frac{f^{(n)}t^{n+1}}{(n+1)!} \right) + \varphi. \quad (42)$$

This phase function is perturbatively expanded at the time origin $t = 0$. Here the index n represents the order of the highest frequency derivative $f^{(n)}$ (different from the associated power index of t^{n+1}).

In this paper, we take the time origin $t = 0$ (for the expansion (42)) at the midpoint of the observational period T . More specifically, we set our observational period by $t \in [-T/2, T/2]$ not by $t \in [0, T]$. As we see below, this choice is for reducing some of the Fisher matrix elements

by a block diagonalization. Applying the Parseval's theorem for a nearly monochromatic signal, we obtain the expected signal-to-noise ratios ρ as

$$\rho^2 = \frac{2}{S_n(f)} \int_{-T/2}^{T/2} h(t)h(t)dt \quad (43)$$

$$= \frac{A^2 T}{S_n(f)} \quad (44)$$

with the effective noise spectrum $S_n(f)$. We have ignored the time dependence of the confusion noise, which will be unimportant at $f \gtrsim 5\text{mHz}$ and $T \gtrsim 4\text{yr}$ [37].

Next, we apply the Fisher matrix analysis to evaluate the measurement errors for the fitting parameters $\theta_n = \{\varphi, f, \dot{f}, \dots, f^{(n)}\}$ in the phase function (42). Note that the error for the amplitude A has no correlation with those for the parameters θ_n . The Fisher matrix elements are formally given as

$$F_{\theta_i \theta_j} = \frac{2}{S_n(f)} \int_{-T/2}^{T/2} \partial_{\theta_i} h(t) \partial_{\theta_j} h(t) dt. \quad (45)$$

We can analytically evaluate these matrix elements and replace the common factor $A^2/S_n(f)$ by ρ^2/T . The covariance matrix $\langle \delta\theta_i \delta\theta_j \rangle$ for the measurement errors $\delta\theta_i$ can be estimated by the inverse of the Fisher matrix as

$$\langle \delta\theta_i \delta\theta_j \rangle = (F^{-1})_{\theta_i \theta_j}. \quad (46)$$

Below, for notational simplicity, we put the rms value of the measurement error by

$$\Delta\theta_i \equiv \langle \delta\theta_i \delta\theta_i \rangle^{1/2}. \quad (47)$$

Here, importantly, the Fisher matrix and its inverse matrix have block diagonal structures. We can divide the parameters θ_n into two subsets, on the basis of the evenness and oddness of the time derivatives (effectively regarding φ as the minus first derivative). The odd ones are $\{\varphi, \dot{f}, \ddot{f}, \dots\}$ and the even ones are $\{f, \dot{f}, \dots\}$. The two groups have no error correlation, owing to the symmetric cancellations in the time integrals (45). For example, we have

$$F_{\varphi \dot{f}} \propto \int_{-T/2}^{T/2} t^3 dt = 0. \quad (48)$$

Here our midpoint expansion plays the critical role.

Our simplified waveform model (41) does not contain other parameters such as the source direction and orientation. In particular, the phase function (42) lacks the Doppler phase modulation induced by the annual rotation of the detector around the Sun. Therefore, one might be skeptical to the validity of our approach. These concerns were closely examined in [12] by comparison of our analytical approach with the full Fisher matrix analysis including other fitting parameters and the Doppler and amplitude modulations [38, 39]. It was shown that,

for observational period $T \gtrsim 2\text{yr}$, our simplified evaluations work quite efficiently for the phase related parameters $\theta_2 = \{\varphi, f, \dot{f}, \ddot{f}\}$. This is because, at $T \gtrsim 2\text{yr}$, we can distinguish the periodic Doppler modulation from the perturbative frequency drift (42) truncated at a finite order. As a result, the mutual correlation between the source geometric parameters and those in Eq. (42) becomes weak, and our simple approach will be valid even for $n = 4$. Note that, For $T \gtrsim 2\text{yr}$, the cancellations similar to Eq. (48) effectively work, even if we include the annual amplitude modulation [12].

B. Analytical Results

In this subsection, for various orders n of the phase expansion, we present the concrete expressions for the estimation errors of the fitting parameters $\theta_n = \{\varphi, f, \dot{f}, \dots, f^{(n)}\}$. As mentioned in the previous subsection, these expressions will be valid for $T \gtrsim 2\text{yr}$.

If the apparent frequency evolution is well described by the second-order expansion $\Phi_2(t)$ with the four parameters $\theta_2 = \{\varphi, f, \dot{f}, \ddot{f}\}$, we can obtain the Fisher matrix results

$$\Delta\varphi = \frac{3}{2\rho}, \quad \Delta f = \frac{5\sqrt{3}}{2\pi\rho T}, \quad \Delta\dot{f} = \frac{6\sqrt{5}}{\pi\rho T^2}, \quad \Delta\ddot{f} = \frac{60\sqrt{7}}{\pi\rho T^3} \quad (49)$$

as presented in [12]. For the third-order expansion $\Phi_3(t)$ with the five fitting parameters $\theta_3 = \{\varphi, f, \dot{f}, \ddot{f}, \overset{\cdot\cdot}{f}\}$ (newly including $\overset{\cdot\cdot}{f}$), we obtain

$$\begin{aligned} \Delta\varphi &= \frac{15}{8\rho}, \quad \Delta f = \frac{5\sqrt{3}}{2\pi\rho T}, \quad \Delta\dot{f} = \frac{21\sqrt{5}}{\pi\rho T^2}, \quad \Delta\ddot{f} = \frac{60\sqrt{7}}{\pi\rho T^3} \\ \Delta\overset{\cdot\cdot}{f} &= \frac{2520}{\pi\rho T^4}. \end{aligned} \quad (50)$$

Because of the block diagonalization, the results $\{\Delta f, \Delta\dot{f}\}$ are the same as those in Eq. (49). In contrast, the remaining ones $\{\Delta\varphi, \Delta\ddot{f}\}$ become larger, reflecting their correlation with the additional error $\Delta\overset{\cdot\cdot}{f}$.

Next we move to the fourth-order function $\Phi_4(t)$ with the six fitting parameters $\theta_4 = \{\varphi, f, \dot{f}, \ddot{f}, \overset{\cdot\cdot}{f}, \overset{\cdot\cdot\cdot}{f}\}$. We obtain

$$\begin{aligned} \Delta\varphi &= \frac{15}{8\rho}, \quad \Delta f = \frac{35\sqrt{3}}{8\pi\rho T}, \quad \Delta\dot{f} = \frac{21\sqrt{5}}{\pi\rho T^2}, \quad \Delta\ddot{f} = \frac{270\sqrt{7}}{\pi\rho T^3} \\ \Delta\overset{\cdot\cdot}{f} &= \frac{2520}{\pi\rho T^4}, \quad \Delta\overset{\cdot\cdot\cdot}{f} = \frac{15120\sqrt{11}}{\pi\rho T^5}. \end{aligned} \quad (51)$$

Here the results $\{\Delta\varphi, \Delta\dot{f}, \Delta\overset{\cdot\cdot}{f}\}$ are the same as those in Eq.(50), but others $\{\Delta f, \Delta\ddot{f}\}$ become larger. In this manner, under the midpoint expansion, we can append the highest derivative coefficients $f^{(n+1)}$ to the fitting parameters, without sacrificing the accuracy of the second highest one $f^{(n)}$. As we see in the next section, this will be preferable at actual data analysis for nearly monochromatic BBHs.

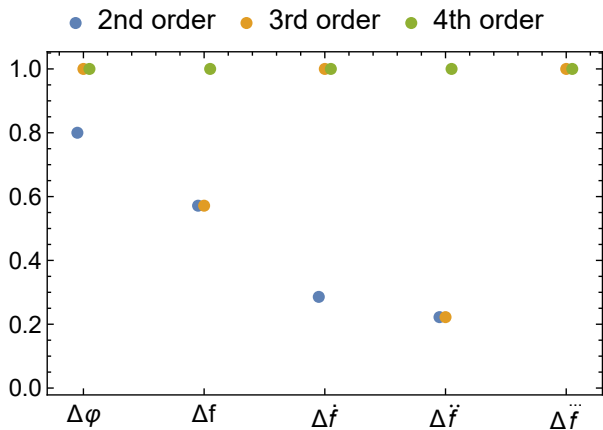


FIG. 2: Comparison of the numerical factors in Eqs. (49)-(51) normalized by those in Eq. (51).

In Fig. 2, to show the dependence on the order of the phase expansion ($n = 2, 3$ and 4), we compare the numerical coefficients for the errors presented in Eqs. (49)-(51) normalized by those presented in Eq. (51). We can see that the lower order parameters such as φ are less affected by the order of the derivative expansion. This seems reasonable, given the differences of the power indexes in the phase function (42).

So far, we have applied the GW phase expansion (42) at the midpoint $t = 0$ of the observation period $[-T/2, T/2]$. For comparison, we evaluated the Fisher matrix results, expanding the GW phase at the initial point $t = 0$ of the integration period $[0, T]$. For the six fitting parameters $\theta_4 = \{\varphi, f, \dot{f}, \ddot{f}, \ddot{f}, \ddot{f}\}$, we obtained

$$\Delta\varphi = \frac{6}{\rho}, \quad \Delta f = \frac{35\sqrt{3}}{\pi\rho T}, \quad \Delta\dot{f} = \frac{336\sqrt{5}}{\pi\rho T^2}, \quad \Delta\ddot{f} = \frac{2160\sqrt{7}}{\pi\rho T^3}$$

$$\Delta\ddot{f} = \frac{25200}{\pi\rho T^4}, \quad \Delta\ddot{f} = \frac{15120\sqrt{11}}{\pi\rho T^5}. \quad (52)$$

The magnitude $\Delta\ddot{f}$ for the highest derivative is identical to Eq. (51) for the midpoint expansion (as explained below), but other parameters have much larger estimation errors. Note that, in the case of the initial point expansion, the diagonal elements $F_{f^{(n)}f^{(n)}}$ of the Fisher matrix (45) are 2^{2n+2} times larger than those for the midpoint expansion (again regarding $\varphi \propto f^{(-1)}$). However, the diagonal elements of the inverted matrix (see Eqs. (46) and (47)) become generally larger for the initial point expansion, as shown in Eqs. (51)-(52). This is due to the off-diagonal elements of the Fisher matrix (related to correlations of the parameters), and the block diagonal structure of the midpoint expansion would play an important role.

Eqs. (51) and (52) are obtained under the assumption that the phase function $\Phi(t)$ is well approximated by the fifth order polynomial expansion of the time variable t . Using the difference of the time origin $t = 0$, we can write down the third derivative coefficient of the initial point

expansion

$$\ddot{f} \simeq \ddot{f}_m - \frac{T}{2} \ddot{f}_m \quad (53)$$

in terms of these evaluated under the midpoint expansion \ddot{f}_m and \ddot{f}_m (temporarily adding the subscript m). Then, we have

$$\Delta\ddot{f} \simeq \left(\Delta\ddot{f}_m^2 + \frac{T^2}{4} \Delta\ddot{f}_m^2 \right)^{1/2} \quad (54)$$

due to the block diagonalization for the midpoint expansion. We can easily confirm the expression $\Delta\ddot{f}$ in (52) from Eq. (51). We also have $\ddot{f} = \ddot{f}_m$ and thus $\Delta\ddot{f} = \Delta\ddot{f}_m$, as commented earlier.

C. Order of the Expansion

In any case, we should carefully adjust the order n of the phase expansion at the matched filtering analysis. An unnecessarily large n results in avoidable degradation of the important parameters such as \dot{f} (see Fig. 2). At the same time, they will be biased, if we take a too small n . In reality, we should adjust the order n , also taking into account the observed properties of the actual BBH samples detected by space detectors. Below, as a working hypothesis, we stop the expansion at the lowest order n satisfying the resolution condition

$$f^{(n)} \lesssim \Delta f^{(n)}. \quad (55)$$

Here, as the reference values, we use the derivatives $f^{(n)}$ given in Eqs. (2)-(5) for radiation reaction. At the next order expansion $n+1$, for our fiducial BBHs, we will have $f^{(n+1)} \ll \Delta f^{(n+1)}$ from the scaling relations $f^{(n)} \propto t_c^{-n}$ and $\Delta f^{(n)} \propto T^{-n+1/2}$, together with the increasingly large numerical factors of the latter (see Eqs. (49)-(51)).

In Fig. 3, assuming circular BBHs and using expressions in Secs. II A and III B, we present the integration time T satisfying the condition $\Delta f^{(n)} = f^{(n)}$ for various chirp masses \mathcal{M} at $f = 5\text{mHz}$. For each index n , we use the error $\Delta f^{(n)}$ obtained with the corresponding expansion $\Phi_n(t)$ (e.g. $\Delta\dot{f}$ from Eq. (49) not from Eq. (51)). We can roughly understand the required order n of the expansion as a function of the integration time T .

In this figure, considering the applicability of our simplified phase model (41), the results will be valid at $T \gtrsim 2$ yr. For the Fisher matrix, we have also used the nearly monochromatic approximation for evaluating the time integrals (45). Therefore, in Fig. 3, we show the time T during which the GW frequency f changes by 1% and 5% (namely $\dot{f}T/f = 0.01$ and 0.05). In Fig. 4, we preset a similar plot, now fixing the chirp mass at $\mathcal{M} = 30M_\odot$.

We have assumed to determine the order n of the Taylor expansion, following the condition (55). This choice is equivalent to set $f^{(n+1)} = f^{(n+2)} = \dots = 0$ for the higher

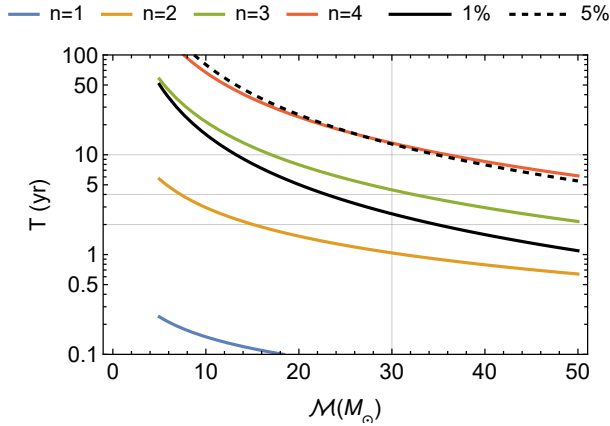


FIG. 3: The integration time T satisfying the condition $\Delta f^{(n)} = f^{(n)}$ at $f = 5\text{mHz}$. The results are given for circular BBHs which have the signal-to-noise ratio $\rho = 10$ in $T = 4\text{yr}$. The GW frequency f changes by 1% and 5% during the time T shown by the black lines.

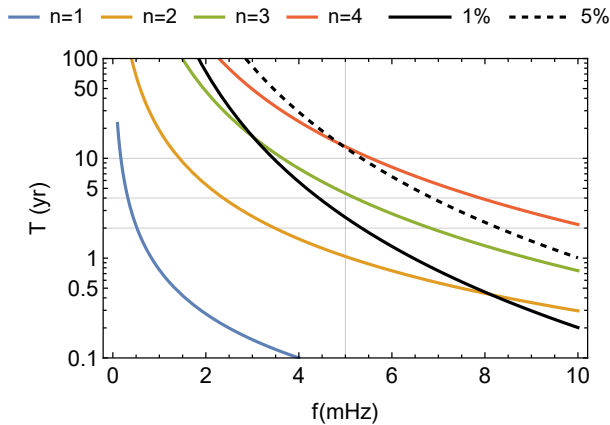


FIG. 4: The integration time T satisfying the condition $\Delta f^{(n)} = f^{(n)}$ at various GW frequency f . The results are given for circular BBHs with the fixed chirp mass $\mathcal{M} = 30M_\odot$ and $\rho = 10$ in $T = 4\text{yr}$. The results at $f = 5\text{mHz}$ are identical to those for $\mathcal{M} = 30M_\odot$ in Fig. 3.

derivative coefficients. The associated phase mismatch is roughly given by

$$\frac{f^{(n+1)}}{(n+2)!} t^{n+2}, \quad (56)$$

which takes the maximum magnitude at the initial and end points $t = \pm T/2$. From the viewpoint of matched filtering analysis, the phase mismatch due to the incomplete template should be much less than unity (see e.g. [40]).

Here we evaluate the integration time T with which the phase mismatch becomes unity as

$$\frac{f^{(n+1)}}{(n+2)!} \left(\frac{T}{2}\right)^{n+2} = 1. \quad (57)$$

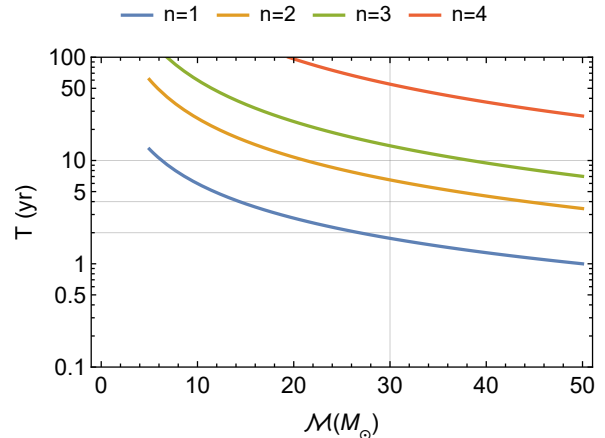


FIG. 5: The integration time T satisfying the condition (57) for the phase mismatch. The results are given for circular BBHs which have the GW frequency $f = 5\text{mHz}$ and various chirp masses \mathcal{M} .

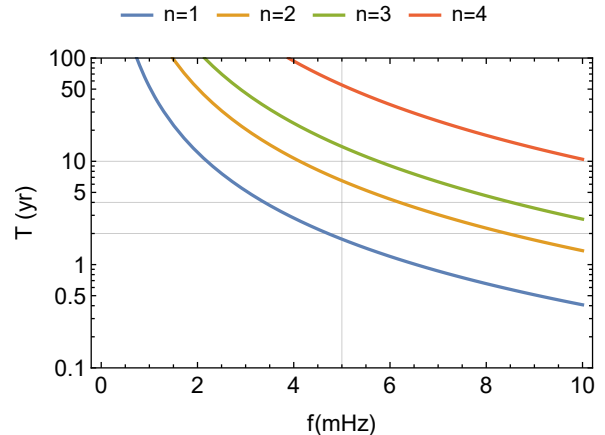


FIG. 6: The integration time T satisfying the condition (57) for the phase mismatch. The results are given for circular BBHs which have the fixed chirp mass $\mathcal{M} = 30M_\odot$ various GW frequencies. The results at $f = 5\text{mHz}$ are identical to those for $\mathcal{M} = 30M_\odot$ in Fig. 5.

The results are presented in Figs. 5 and 6. Comparing Figs. 3 and 5, we can see that, for a given n (e.g. $n = 3$), the integration time T in Fig. 3 is generally smaller than that in Fig. 5. Therefore, following the condition (55), the associated phase mismatch will be much less than unity. We can confirm similar results in Figs. 4 and 6. We should also note that the left-hand side of Eq. (57) is proportional to $f^{(n+1)}T^{(n+2)}$, in a similar way to the ratio $f^{(n+1)}/(\Delta f^{(n+1)})$.

IV. OBSERVATIONAL PROSPECTS

We now discuss the prospects for measuring the frequency derivatives for our fiducial BBH. For a circular

orbit, from Eqs. (2)-(5) (also Table I), we have

$$\dot{f} = 6.2 \times 10^{-13} \text{Hz s}^{-1}, \quad (58)$$

$$\ddot{f} = 2.8 \times 10^{-22} \text{Hz s}^{-2}, \quad (59)$$

$$\dddot{f} = 2.2 \times 10^{-31} \text{Hz s}^{-3}, \quad (60)$$

$$\dots f = 2.4 \times 10^{-40} \text{Hz s}^{-4}. \quad (61)$$

Below, also for mildly eccentric BBHs ($e \lesssim 0.1$), we use these results as the reference values.

In this section, we mainly set $T = 4$ yr and $\rho = 10$, given the nominal operation period of LISA. In section IV D, we discuss the case for an extended case $T = 10$ yr and $\rho = (10/4)^{1/2} \times 10 \simeq 16$.

A. Estimation Errors

Using expressions (49) for the second order phase expansion $\Phi_2(t)$, we obtain

$$\Delta \dot{f} = 2.7 \times 10^{-17} \text{Hz s}^{-1} \quad (62)$$

$$\Delta \ddot{f} = 2.5 \times 10^{-24} \text{Hz s}^{-2} \quad (63)$$

for $\rho = 10$ and $T = 4$ yr. Given the relation $\Delta \ddot{f} \ll \ddot{f}$ for the highest derivative \ddot{f} (presented in Eq. (59)), we examine the next-order function $\Phi_3(t)$. From expression (50), we obtain

$$\Delta \dot{f} = 9.4 \times 10^{-17} \text{Hz s}^{-1} \quad (64)$$

$$\Delta \ddot{f} = 2.5 \times 10^{-24} \text{Hz s}^{-2} \quad (65)$$

$$\Delta \ddot{f} = 3.2 \times 10^{-31} \text{Hz s}^{-3}. \quad (66)$$

Now we have a relation $\ddot{f} \lesssim \Delta \ddot{f}$ for the highest derivative. As shown in Eqs. (63) and (65), due to the block diagonalization, the error $\Delta \dot{f}$ is invariant. In contrast, the error $\Delta \dot{f}$ in Eq. (64) becomes 7/2 times larger than that in Eq. (62). We still have $\Delta \dot{f} \ll \dot{f}$ and this degradation of the factor 7/2 might not be a practical problem from astrophysical point of views. This is because we usually do not need to very accurately (sub-percent level) measure the rate \dot{f} (or the redshifted chirp mass) alone. When we extract some astrophysical information by combining the rate \dot{f} with other fitting parameters (e.g. \dot{f} for the combination C_2 as discussed in section II B), the error $\Delta \dot{f}$ will have a minor contribution to the total error.

Using Eq. (51) for the fourth-order expansion $\Phi_4(t)$, we have the estimation errors

$$\Delta \dot{f} = 9.4 \times 10^{-17} \text{Hz s}^{-1} \quad (67)$$

$$\Delta \ddot{f} = 1.1 \times 10^{-23} \text{Hz s}^{-2} \quad (68)$$

$$\Delta \ddot{f} = 3.2 \times 10^{-31} \text{Hz s}^{-3} \quad (69)$$

$$\Delta \dots f = 5.0 \times 10^{-38} \text{Hz s}^{-4}. \quad (70)$$

We now have $\ddot{f} \ll \Delta \ddot{f}$ for the highest derivative, and this expansion will be excessive in view of the criteria (55), hampering the resolution $\Delta \dot{f}$ (increased by a factor of 9/2 from Eq. (65)). The reasonable choice will be $n = 3$, and we below use Eqs. (64)-(66) for the estimation errors.

B. Eccentricity Estimation

We next discuss the extraction of the astrophysical information from the observed products C_n .

Given the hierarchy of the relative errors $\Delta f^{(n)}/f^{(n)}$, the measurement error ΔC_n is estimated to be

$$\Delta C_n \sim \frac{\Delta C_n}{C_n} \sim \frac{\Delta f^{(n)}}{f^{(n)}} \quad (71)$$

up to moderate eccentricity with $C_n \sim 1$. For our fiducial BBH, from Eqs. (59) and (65), we have $\Delta C_2 \sim 9 \times 10^{-3}$. With the relation $\Delta \dot{f} \sim \dot{f}$ for the next order one C_3 , we cannot measure C_3 in real terms. In addition, even for the reference system in Sec. II C, the shift of C_2 due to the tertiary is comparable to its error ΔC_2 . Therefore, below in this subsection, we concentrate on the eccentricity measurement from the product C_2 .

If the observed value C_2 is consistent with unity (namely $|C_2 - 1| \lesssim \Delta C_2$), we can apply Eq. (20) and set an upper limit to the eccentricity as

$$e \lesssim \left\{ \frac{792}{2983} \Delta C_2 \right\}^{1/2}. \quad (72)$$

We have $e \lesssim 0.05$ for our fiducial BBH.

In contrast, if the product C_2 satisfies the condition $C_2 - 1 \gg \Delta C_2$, we can solve Eq. (19) for the eccentricity e with the estimation error

$$\Delta e \sim \frac{\Delta C_2}{|\partial_e K_2(e)|}. \quad (73)$$

As an example, for the true value $e = 0.1$, we have $C_2 = K_2(0.1) = 0.96$, and the expected estimation error becomes $\Delta e \sim 1.3 \times 10^{-2}$.

C. Extension to 10yr

In this subsection, we discuss the results for an extended observation of $T = 10$ yr. Compared with $T = 4$ yr, the signal-to-noise ρ increases by a factor of $2.5^{1/2} \sim 1.6$ and the estimation errors $\Delta f^{(n)}$ formally shrink by $0.4^{n+3/2}$ (0.1 for $n = 2$, 0.016 for $n = 3$ and 0.006 for $n = 4$). However, for a longer T , we need to increase the order n of the phase expansion, following the criteria (55). Therefore, these scaling factors cannot be simply applicable.

For the third-order phase function $\Phi_3(t)$, from Eq. (50), we have the estimation errors

$$\Delta \dot{f} = 9.5 \times 10^{-18} \text{Hz s}^{-1} \quad (74)$$

$$\Delta \ddot{f} = 1.0 \times 10^{-25} \text{Hz s}^{-2} \quad (75)$$

$$\Delta \ddot{f} = 5.2 \times 10^{-33} \text{Hz s}^{-3} \quad (76)$$

TABLE II: The resolutions for the frequency derivatives at $T = 4$ and 10 yr (respectively from Eqs. (64)-(66) and Eqs. (77)-(80)).

T	4yr	10yr	ratio
$\Delta \dot{f}$	$9.4 \times 10^{-17} \text{Hz s}^{-1}$	$9.5 \times 10^{-18} \text{Hz s}^{-1}$	0.10
$\Delta \ddot{f}$	$2.5 \times 10^{-24} \text{Hz s}^{-2}$	$4.6 \times 10^{-25} \text{Hz s}^{-2}$	0.18
$\Delta \dddot{f}$	$3.2 \times 10^{-31} \text{Hz s}^{-3}$	$5.2 \times 10^{-33} \text{Hz s}^{-3}$	0.016
$\Delta \ddot{\ddot{f}}$		$3.3 \times 10^{-40} \text{Hz s}^{-4}$	

with $\Delta \ddot{\ddot{f}} \ll \ddot{\ddot{f}}$ for the highest derivative. Similarly, from Eq. (51) for the function $\Phi_4(t)$ we obtain

$$\Delta \dot{f} = 9.5 \times 10^{-18} \text{Hz s}^{-1} \quad (77)$$

$$\Delta \ddot{f} = 4.6 \times 10^{-25} \text{Hz s}^{-2} \quad (78)$$

$$\Delta \ddot{\ddot{f}} = 5.2 \times 10^{-33} \text{Hz s}^{-3} \quad (79)$$

$$\Delta \ddot{\ddot{\ddot{f}}} = 3.3 \times 10^{-40} \text{Hz s}^{-4} \quad (80)$$

now with the desired relation $\ddot{\ddot{f}} \lesssim \Delta \ddot{\ddot{f}}$. Below, we use the estimation errors in Eq. (77)-(80). In Table II, we compare these results with those estimated for $T = 4$ yr. Because of the block diagonal structure, we can significantly improve the resolution $\Delta \dot{f}$ with the full scaling relation $0.4^{9/2}$ mentioned before.

The error $\Delta \dot{f}$ for $T = 10$ yr is 5 times smaller than that for $T = 4$ yr. We then have

$$\Delta C_2 \sim \frac{\Delta \dot{f}}{\dot{f}} \sim 1.6 \times 10^{-3}, \quad (81)$$

and the PN effects are likely to be still unresolvable. However, for a larger chirp mass \mathcal{M} and a higher frequency f , the PN effects should be taken into account.

From Eqs. (60) and (79), we can evaluate the estimation error for C_3

$$\Delta C_3 \sim \frac{\Delta \ddot{\ddot{f}}}{\ddot{\ddot{f}}} \sim 2.4 \times 10^{-2}. \quad (82)$$

As expected, we have $\Delta C_3 \gg \Delta C_2$.

D. Tertiary Signatures

Now, based on the results for $T = 10$ yr, we discuss the search for the tertiary effect. For a nearly circular BBH perturbed by the reference tertiary model in Sec. II C, we have

$$C_2 - 1 \simeq \frac{\ddot{f}_s}{\dot{f}_r} \simeq -6.0 \times 10^{-3} \sin \psi_s, \quad (83)$$

which becomes incompatible with an isolated BBH for $\sin \psi_s < 0$. The excess can be measured with the resolution ΔC_2 given in Eq. (81), and we can detect it at 3.6σ for the optimal phase $\sin \psi_s = -1$ (corresponding to $\ddot{f}_s \sim 2 \times 10^{-24} \text{Hz s}^{-2}$). For $T = 4$ yr, the same excess

will be totally masked by the measurement noise with $|C_2 - 1| \ll \Delta C_2$.

Next, for an eccentric binary, we can examine the inconsistency between C_2 and C_3 induced by the tertiary perturbation. In fact, given the condition $\Delta C_3 \gg \Delta C_2$, it will be more straightforward to compare C_3 and the corresponding value $K_3[K_2^{-1}(C_2)]$. The uncertainty ΔC_3 dominates the statistical error for the gap between them. From Eqs. (36) and (38), the gap is approximately estimated to be

$$C_3 - K_3[K_2^{-1}(C_2)] \simeq \frac{\ddot{f}_s}{\dot{f}_r} \simeq -2.6 \times 10^{-2} \cos \psi_s. \quad (84)$$

Given the uncertainty (82), the third derivative \ddot{f}_s (due to the reference tertiary perturbation) can be detected only at 1σ level, even for the optimal orbital phase $|\cos \psi_s| = 1$.

V. DISCUSSIONS

Here are some additional remarks regarding our current investigation.

A. Other Harmonic Modes

So far, we have mainly discussed observation for GW around a single frequency f (twice the orbital frequency). An eccentric binary emits GWs at integer times the orbital frequency. Up to a moderate eccentricity $e \lesssim 0.3$, the third harmonic mode at the frequency $3f/2$ will be the secondary target, and its amplitude is proportional to e with its SNR $\sim \rho e$ (ρ : the SNR of the primary mode). As argued in [15, 41], by closely analyzing the signatures induced by the 1PN apsidal precession on the third harmonics, we might determine the total mass M_T of the BBH.

For our fiducial BBH ($\rho \sim 10$ and $f \sim 5$ mHz), the third harmonics is detectable for $e \sim 0.3$, and we can estimate the orbital eccentricity e from the amplitude of the mode. Unfortunately, the resultant error Δe will be much larger than that from C_2 as discussed in Eq. (73). However, in the lower frequency regime e.g. $f \sim 1$ mHz, we cannot measure the second derivative \dot{f} (see Fig. 4), and the third harmonics could be a relatively better target.

B. Long-term Noise Variation

For the block diagonalization associated with the mid-point expansion, we have assumed that the effective noise spectrum $S_n(f)$ does not depend on time (more precisely, during the course of the matched filtering analysis). In practice, detectors may degrade over time, and we might also operate a network consisting of multiple detectors (e.g., LISA+Taiji [42]) functioning at different

time intervals. In such scenarios, we cannot straightforwardly apply the odd-even cancellation (48) based solely on the stationarity of the noise $S_n(f)$. However, we can still adjust the time origin $t = 0$ for the perturbative phase expansion and achieve similar (but more restricted) features to the structure of the Fisher matrix.

VI. SUMMARY

LISA has a potential to detect stellar mass BBHs, which are similar to those already observed by ground-based detectors. According to a recent statistical study [7], the majority of the detected BBHs will emit nearly monochromatic GWs, exhibiting slight frequency variations within the nominal operational period of $T \sim 4$ years. To characterize such signals, we can efficiently employ a Taylor expansion for the evolution of the GW frequency f . The associated derivative coefficients, such as \dot{f} and \ddot{f} , may harbor intriguing astrophysical information, such as orbital eccentricity and tertiary perturbation effects. To facilitate this analysis, we introduced non-dimensional measures C_n ($n = 2, 3, \dots$) with $C_n = 1$ for an isolated circular binary.

We provided simple analytical expressions for the parameter estimation errors for the derivatives $f^{(n)}$, applying the Fisher matrix formulation to a simplified phase model $\Phi_n(t)$. Then, we concretely discuss the measurability of the aforementioned astrophysical information for our fiducial BBH (chirp mass $\mathcal{M} \sim 30M_\odot$, the GW frequency $f \sim 5\text{mHz}$ and the signal-to-noise ratio $\rho = 10$ for $T = 4\text{yr}$). We found that LISA can make a resolution $\Delta C_2 \sim \Delta \ddot{f}/\ddot{f} \sim 10^{-2}$, corresponding to the eccentricity error $\Delta e \sim 1.3 \times 10^{-2}$ for $e = 0.1$. For an extended operation period of $T \sim 10\text{yr}$, we might also make the next order combination C_3 and detect a tertiary perturbation as small as $\dot{f}_s \sim 2 \times 10^{-24}\text{Hz s}^{-2}$ for a nearly circular BBH.

Acknowledgments

Equation (15) plays an important role in this paper. The author is deeply grateful to Tomoya Suzuguchi for pointing out errors in its previous version.

-
- [1] R. Abbott *et al.* [KAGRA, VIRGO and LIGO Scientific], Phys. Rev. X **13**, no.4, 041039 (2023) doi:10.1103/PhysRevX.13.041039 [arXiv:2111.03606 [gr-qc]].
- [2] P. Amaro-Seoane *et al.* [LISA], [arXiv:1702.00786 [astro-ph.IM]].
- [3] W. H. Ruan, Z. K. Guo, R. G. Cai and Y. Z. Zhang, Int. J. Mod. Phys. A **35**, no.17, 2050075 (2020) doi:10.1142/S0217751X2050075X [arXiv:1807.09495 [gr-qc]].
- [4] J. Luo *et al.* [TianQin], Class. Quant. Grav. **33**, no.3, 035010 (2016) doi:10.1088/0264-9381/33/3/035010 [arXiv:1512.02076 [astro-ph.IM]].
- [5] P. Amaro-Seoane *et al.* [LISA], Living Rev. Rel. **26** (2023) no.1, 2 doi:10.1007/s41114-022-00041-y [arXiv:2203.06016 [gr-qc]].
- [6] A. Sesana, Phys. Rev. Lett. **116**, no.23, 231102 (2016) doi:10.1103/PhysRevLett.116.231102 [arXiv:1602.06951 [gr-qc]].
- [7] N. Seto and K. Kyutoku, Mon. Not. Roy. Astron. Soc. **514**, no.4, 4669-4675 (2022) doi:10.1093/mnras/stac1561 [arXiv:2201.02766 [astro-ph.HE]].
- [8] D. Gerosa, S. Ma, K. W. K. Wong, E. Berti, R. O’Shaughnessy, Y. Chen and K. Belczynski, Phys. Rev. D **99**, no.10, 103004 (2019) doi:10.1103/PhysRevD.99.103004 [arXiv:1902.00021 [astro-ph.HE]].
- [9] A. Klein, G. Pratten, R. Busicchio, P. Schmidt, C. J. Moore, E. Finch, A. Bonino, L. M. Thomas, N. Williams and D. Gerosa, *et al.* [arXiv:2204.03423 [astro-ph.HE]].
- [10] T. E. Strohmayer 2021, ApJL, 912, L8. doi:10.3847/2041-8213/abf3cc
- [11] J. Munday, T. R. Marsh, M. Hollands, I. Pelisoli, D. Steeghs, P. Hakala, E. Breedt, A. Brown, V. S. Dhillon and M. J. Dyer, *et al.* Mon. Not. Roy. Astron. Soc. **518** (2022) no.4, 5123-5139 doi:10.1093/mnras/stac3385 [arXiv:2211.09834 [astro-ph.SR]].
- [12] N. Seto, Phys. Rev. D **108**, no.2, 023019 (2023) doi:10.1103/PhysRevD.108.023019 [arXiv:2307.04453 [gr-qc]].
- [13] R. Ebadi, V. Stokov, E. H. Tanin, E. Berti and R. L. Walsworth, [arXiv:2405.13109 [gr-qc]].
- [14] P. C. Peters, Phys. Rev. **136**, B1224-B1232 (1964) doi:10.1103/PhysRev.136.B1224
- [15] N. Seto, Mon. Not. Roy. Astron. Soc. **460**, no.1, L1-L4 (2016) doi:10.1093/mnras/lslw060 [arXiv:1602.04715 [astro-ph.HE]].
- [16] A. Nishizawa, A. Sesana, E. Berti and A. Klein, Mon. Not. Roy. Astron. Soc. **465**, no.4, 4375-4380 (2017) doi:10.1093/mnras/stw2993 [arXiv:1606.09295 [astro-ph.HE]].
- [17] N. Seto, Astrophys. J. Lett. **677**, L55-L58 (2008) doi:10.1086/587785 [arXiv:0802.3411 [astro-ph]].
- [18] N. Seto and K. Kyutoku, Phys. Rev. Lett. **118**, no.15, 151101 (2017) doi:10.1103/PhysRevLett.118.151101 [arXiv:1611.05875 [astro-ph.HE]].
- [19] N. Tamanini and C. Danielski, Nature Astron. **3**, no.9, 858-866 (2019) doi:10.1038/s41550-019-0807-y [arXiv:1812.04330 [astro-ph.EP]].
- [20] K. W. K. Wong, V. Baibhav and E. Berti, Mon. Not. Roy. Astron. Soc. **488**, no.4, 5665-5670 (2019) doi:10.1093/mnras/stz2077 [arXiv:1902.01402 [astro-ph.HE]].
- [21] Y. Kang, C. Liu and L. Shao, Astron. J. **162**, no.6, 247 (2021) doi:10.3847/1538-3881/ac23d8 [arXiv:2108.01357]

- [astro-ph.EP]].
- [22] T. Robson, N. J. Cornish, N. Tamanini and S. Toonen, *Phys. Rev. D* **98**, no.6, 064012 (2018) doi:10.1103/PhysRevD.98.064012 [arXiv:1806.00500 [gr-qc]].
- [23] Z. Xuan, P. Peng, X. Chen, 2021, *MNRAS*, 502, 4199. doi:10.1093/mnras/stab331
- [24] F. Zhang, X. Chen, L. Shao and K. Inayoshi, *Astrophys. J.* **923**, no.2, 139 (2021) doi:10.3847/1538-4357/ac2c07 [arXiv:2109.14842 [astro-ph.HE]].
- [25] K. i. Maeda, P. Gupta and H. Okawa, *Phys. Rev. D* **107**, no.12, 124039 (2023) doi:10.1103/PhysRevD.107.124039 [arXiv:2303.16553 [gr-qc]].
- [26] N. Tamanini, A. Klein, C. Bonvin, E. Barausse and C. Caprini, *Phys. Rev. D* **101**, no.6, 063002 (2020) doi:10.1103/PhysRevD.101.063002 [arXiv:1907.02018 [astro-ph.IM]].
- [27] T. Takahashi, H. Omiya and T. Tanaka, *Phys. Rev. D* **107**, no.10, 103020 (2023) doi:10.1103/PhysRevD.107.103020 [arXiv:2301.13213 [gr-qc]].
- [28] L. Blanchet, *Living Rev. Rel.* **17**, 2 (2014) doi:10.12942/lrr-2014-2 [arXiv:1310.1528 [gr-qc]].
- [29] C. Cutler and E. E. Flanagan, *Phys. Rev. D* **49**, 2658-2697 (1994) doi:10.1103/PhysRevD.49.2658 [arXiv:gr-qc/9402014 [gr-qc]].
- [30] M. Punturo, M. Abernathy, F. Acernese, B. Allen, N. Andersson, K. Arun, F. Barone, B. Barr, M. Barsuglia and M. Beker, *et al. Class. Quant. Grav.* **27**, 194002 (2010) doi:10.1088/0264-9381/27/19/194002
- [31] S. Tanay, M. Haney and A. Gopakumar, *Phys. Rev. D* **93**, no.6, 064031 (2016) doi:10.1103/PhysRevD.93.064031 [arXiv:1602.03081 [gr-qc]].
- [32] N. Seto, *Mon. Not. Roy. Astron. Soc.* **524**, no.4, 5442-5445 (2023) doi:10.1093/mnras/stad2187 [arXiv:2307.09739 [astro-ph.HE]].
- [33] C. G. Bassa, G. H. Janssen, B. W. Stappers, T. M. Tauris, T. Wevers, P. G. Jonker, L. Lentati, J. P. W. Verbiest, G. Desvignes and E. Graikou, *et al. Mon. Not. Roy. Astron. Soc.* **460**, no.2, 2207-2222 (2016) doi:10.1093/mnras/stw1134 [arXiv:1604.00129 [astro-ph.HE]].
- [34] D. L. Kaplan, T. Kupfer, D. J. Nice, A. Irrgang, U. Heber, Z. Arzoumanian, E. Beklen, K. Crowter, M. E. DeCesar and P. B. Demorest, *et al. Astrophys. J.* **826**, no.1, 86 (2016) doi:10.3847/0004-637X/826/1/86 [arXiv:1604.00131 [astro-ph.HE]].
- [35] J. Samsing, K. Hendriks, L. Zwick, D. J. D'Orazio and B. Liu, [arXiv:2403.05625 [astro-ph.HE]].
- [36] N. Seto, *Mon. Not. Roy. Astron. Soc.* **333**, 469 (2002) doi:10.1046/j.1365-8711.2002.05432.x [arXiv:astro-ph/0202364 [astro-ph]].
- [37] T. Robson, N. J. Cornish and C. Liu, *Class. Quant. Grav.* **36**, no.10, 105011 (2019) doi:10.1088/1361-6382/ab1101 [arXiv:1803.01944 [astro-ph.HE]].
- [38] R. Takahashi and N. Seto, *Astrophys. J.* **575**, 1030-1036 (2002) doi:10.1086/341483 [arXiv:astro-ph/0204487 [astro-ph]].
- [39] C. Cutler, *Phys. Rev. D* **57**, 7089-7102 (1998) doi:10.1103/PhysRevD.57.7089 [arXiv:gr-qc/9703068 [gr-qc]].
- [40] J. D. E. Creighton and W. G. Anderson, *Gravitational-wave physics and astronomy: An introduction to theory, experiment and data analysis* (2011).
- [41] N. Seto, *Phys. Rev. Lett.* **87**, 251101 (2001) [erratum: *Phys. Rev. Lett.* **101**, 209901 (2008)] doi:10.1103/PhysRevLett.87.251101 [arXiv:astro-ph/0111107 [astro-ph]].
- [42] R. G. Cai, Z. K. Guo, B. Hu, et al., [arXiv:2305.04551 [gr-qc]].